Recent tangible interannual variability of monsoonal orographic rainfall in the Eastern Himalayas

Pratik Kad[1] and Kyung-Ja Ha[1]

[1]Pusan National University

November 27, 2023

Abstract

Himalayas hydroclimate is a lifeline for South Asia's most densely populated region. Every year flooding in the Himalayan rivers is usual during monsoon, which impacts millions of inhabitants of the Himalayas and downstream regions. Recent studies demonstrate the role of melting glaciers and snow, in the context of global warming, along with monsoonal rain causing recurrent floods. Here, we highlight the interannual variability in the eastern Himalayan hydroclimate as a natural hazard using observed reanalysis for the last 43 years (1979-2021). We found anomalous extreme years with eight dry years and eight wet years after removing the climate change signal. Monsoon rainfall is a significant contributor, and melting snow is not a potential contributor to these anomalous extreme years. The variability of Himalayan monsoonal rainfall is strongly regulated by local monsoonal Hadley circulation associated with Walker circulation. Our findings demonstrate mechanisms associated with Himalayan wet and dry response. The insights provided in this study underscore the impact of natural variability-driven challenging events that could be predictable. Thus, this mechanism could improve the predictability of the Himalayas floods.

Hosted file

952499_0_art_file_10569222_rnjhxd.docx available at https://authorea.com/users/499715/articles/617475-recent-tangible-interannual-variability-of-monsoonal-orographic-rainfall-in-the-eastern-himalayas

Recent tangible interannual variability of monsoonal orographic rainfall in the Eastern Himalayas

Pratik Kad[1], and Kyung-Ja Ha[1,2,3]

[1]Department of Climate System, Pusan National University, Busan, South Korea

[2]Center for Climate Physics, Institute for Basic Science, Busan, South Korea

[3]BK21 School of Earth and Environmental Systems, Pusan National University, Busan, South Korea

*Corresponding author: Kyung-Ja Ha (kjha@pusan.ac.kr)

Key Points:

- This study extends our understanding of natural variability across the Eastern Himalayan steep orography using reanalysis data.
- Composite analysis reveals that orographic siege strongly modulates moisture flux convergence, resulting in wet and arid events.
- This study can be helpful in the predictability of recurrent Himalayas floods.

Abstract

Himalayas hydroclimate is a lifeline for South Asia's most densely populated region. Every year flooding in the Himalayan rivers is usual during monsoon, which impacts millions of inhabitants of the Himalayas and downstream regions. Recent studies demonstrate the role of melting glaciers and snow, in the context of global warming, along with monsoonal rain causing recurrent floods. Here, we highlight the interannual variability in the eastern Himalayan hydroclimate as a natural hazard using observed reanalysis for the last 43 years (1979-2021). We found anomalous extreme years with eight dry years and eight wet years after removing the climate change signal. Monsoon rainfall is a significant contributor, and melting snow is not a potential contributor to these anomalous extreme years. The variability of Himalayan monsoonal rainfall is strongly regulated by local monsoonal Hadley circulation associated with Walker circulation. Our findings demonstrate mechanisms associated with Himalayan wet and dry response. The insights provided in this study underscore the impact of natural variability-driven challenging events that could be predictable. Thus, this mechanism could improve the predictability of the Himalayas floods.

1 Introduction

The Himalayas are essential to the global water cycle(Immerzeel et al., 2020). It also holds the most dominant biodiversity hotspots in the Himalayan ranges, including natural heritage like Chitwan National Park, Kaziranga National Park, Khangchendzonga National Park, Manas Wildlife Sanctuary, etc. The Himalayas is one of the most young mountain range on Earth, which emerged around 50 million years ago, resulting from a continental collision according to plate tectonics(Besse et al., 1984; Yin, 2006). These mountain ranges penetrate the atmosphere and regulate monsoonal circulation(Sandu et al., 2019), tropical easterly jets, and river systems. The Intergovernmental Panel on Climate Change (IPCC) special report about the cryosphere has pointed out that the Himalayan snow cover has reduced, and their glaciers underwent substantial ice loss during the last half-decade (Hock et al., 2019; Maurer et al., 2019; Shukla & Sen, 2021).

Previous studies predominantly concentrated over the Tibetan Plateau and its warming (e.g. (Guo et al., 2021, 2016; Rangwala et al., 2009)). On the other hand, studies on the Himalayan hydroclimate and its variability are limited, which is an essential aspect of the Indian subcontinent. Himalayan range comes under the Indian Monsoon framework, which is intensively studied and the most eminent domain of the global monsoon system. Northeast India gets the highest rainfall during Indian monsoon analogized to any other part of Indian subcontinent(Mahanta et al., 2013). This region also includes Cherrapunji and Mawsynram, reportedly the wettest place on Earth(Kuttippurath et al., 2021). Indian monsoon has different flavors such as decadal, interannual, annual, semi-annual, seasonal, and diurnal. Rainfall over the south-facing terrain of the Himalayas is distinguished by an orographic diurnal cycle(Bhatt and

Nakamura, 2006; Hunt et al., 2022). However, a recent study highlights drying due to amplification in the diurnal cycle(Norris et al., 2020). Additionally, the analysis also confirmed the rising temperature over the Himalayas(Pepin et al., 2015; Sabin et al., 2020), along with decreasing trend in monsoon rainfall(Mathew Koll Roxy et al., 2015). These all pointed to the minor role of monsoon and multi-year flooding that might be attributed to ice loss and snow melting.

Summer monsoon representation employing global climate models over the Himalayas and downstream regions is still challenging(Palazzi et al., 2015; Pathak et al., 2019; Salunke et al., 2018). Here, we preferred reanalysis data as rainfall observation reliability across mountainous regions is limited(Hock et al., 2019; Zandler et al., 2019) due to less spatial coverage of situ measurement. Also, ERA5(Hersbach et al., 2020) shows a more acceptable spatial pattern of observed precipitation over the southern central Himalayas than available coarse resolution datasets(Chen et al., 2021). This analysis intends to disentangle the interannual linkage between anomalous rainfall in the Himalayas and underline mechanisms.

2 Materials and Methods

2.1 Data

We use atmospheric variables at 0.25° horizontal resolution from the European Center for Medium Range Weather Forecasting (ECMWF) reanalysis ERA5(Hersbach et al., 2020) for 1979–2021. Sea surface temperature from ERA5 is similar to HadSST obtained from the Met Office Hadley centre, and we thus only use ERA5 in our analyses for consistency. The topography elevation at a five-minute grid resolution (etopo5) is obtained from NASA. Daily MSWEP(Beck et al., 2019) rainfall product data with 0.1° x 0.1° horizontal resolution obtained from GloH_2O. Daily mean river discharge at 0.1° x 0.1° horizontal resolution reanalysis data downloaded from GloFAS-ERA5(Harrigan et al., 2020) reanalysis. The global population density estimates in 2020 from the Gridded Population of the World(CIESIN, 2018) at a resolution of 15 arc-minute (approx. 30km).

2.2 Methodology

We are motivated to explore monsoonal flooding over the Himalayas in the context of natural variability. First, we considered detrended anomalies at each grid point in order to remove the influence of the annual climatological cycle, along with the linear global warming trend. Then we removed externally forced low-frequency variability using a high-pass filter to isolate the interdecadal variability. The result is similar even if using bandpass filtering for interannual to the quasi-decadal window (at 2-13 years). The variability is computed by taking the standard deviation of the filtered time window. Then, we have chosen a high variability amplitude region for futhur analysis when the grid points exceed the amplitude threshold of 4 mm per day, as shown in Fig.1(b).

2.2.1 Moisture flux convergence

We computed the three-dimensional Moisture flux convergence (MFC) as it can tell more about topographic features. The horizontal MFC can be expressed as follow:

$$MFC = -\nabla.(qV_h)$$

Where $V_h(u, v)$ is horizontal wind velocity; u and v are the zonal and meridional components of the wind.

Furthermore, Anomalous MFC can be decomposed into dynamical MFC and thermodynamical MFC. Delta indicates the anomaly with reference to mean state climatology.

$$\Delta\left(-\nabla.(qV_h)\right) = -\nabla.(\overline{q}\Delta V_h) - \nabla.\left(\Delta q\overline{V_h}\right)$$

2.2.2 Local Hadley circulation

We consider the mass stream function (Peixto & Oort, 1984) to understand the mean local meridional circulation. The local meridional mass stream function is expressed as follows:

$$\Psi = \frac{2\pi\, a \cos\phi}{g} \int_{p}^{p_s} \vec{V}\, dp$$

Where a is the Earth's radius, and ϕ is latitude, g is the acceleration due to gravity, V is the zonal mean meridional velocity, p is the pressure, and Ps is the surface pressure.

4 Results

Himalayan rainfall distribution mainly depends on moisture availability via southwest monsoon flow and earns massive rainfall during the summer monsoon season (JJAS). Floods and droughts regularly occur in the monsoon zone, and eventually thosecause socio-economic consequences. Traditionally, the land-sea thermal contrast is a primary physical mechanism that drives monsoon circulation. When this moist wind is lifted over the Himalayas and mountain ranges, it cools and condensates in the form of orographic rainfall. Synoptic features are complicated on the spatial and temporal scale over Himalayan regions due to complex elevation topography and characterized by the steep gradient (Fig.1a and b). Himalaya is the source of earth's major rivers, the Ganges and Brahmaputra, essential water resources for the Indian subcontinent, which also provides irrigation and transportation in a densely populated region (Fig.1c). The Himalayan Rivers flooded yearly during the monsoon season, especially the Brahmaputra. Thus, an advanced early warning system in the Himalayan ranges is necessary for policymakers and stakeholders. Mean monsoon rainfall climatology (Fig. 2a) dominates in the steep mountain ranges and monopolizes from west to east, due to orographic lifting by the orographic blocking effect. However, more orographic rainfall spread can be seen over Eastern Himalayas due to its unique orientation. The linear trend in rainfall (Fig. 2b) shows the tripolar pattern, a slight decline over the Western Himalayas, an increasing pattern over the central Himalayas peripheral to the Ganges basin, and a strong reduction in orographic rainfall over the

eastern Himalayas in the vicinity of Brahmaputra basin. Interestingly, monsoonal variability (Fig. 3c) is also substantial over a steep Himalayan range, similar to its climatology feature.

In order to confirm interannual single in hydroclimate over the Himalayan region, we used bandpass of 2-8 years for detrended anomalies, which show evident variability patterns (Fig. 3a and b) in surface runoff and rainfall in the Himalayan range. The Eastern Himalayas region holds high variability and is dominated by steep topographic elevation. The considerable rainfall variations over this region are highly associated with flooding and arid events. For composite analysis (see methods and Fig.3c), we found eight wet years (1984, 1993, 1995, 1998, 2004, 2007, 2010, and 2020) and eight dry years (1981, 1986, 1992, 1994, 2001, 2006, 2011, and 2013) from interannual scale pinpointed based on multi-year standard deviation over last 43 years (1979-202). To further understand the variability of Himalayan rainfall, we look at composite maps for wet and dry years. Anomalous rainfall patterns are almost identical and heightened in the eastern Himalayas, showing consistent signs in wet and dry years (Fig. 4a and b). A similar feature is replicated in river discharge anomalies (Fig. 4c and d); river discharge is the volume of water streaming through a river routing. Here, Ganges and Brahmaputra show a tight relationship with Himalayan high rainfall variability region. Rainfall anomlies is responsible for runoff, which can further aggravate river floods hazard(Jian et al., 2009). Brahmaputra river flooding years are matching a previous study (see ref (Jian et al., 2009; Rao et al., 2020)) reflecting the role of natural climate variability. However, we can see it's not just limited to the Brahmaputra basin, and it can be considered as the whole Himalayan reserve system. The anomalous surface runoff pattern follows a steep southeast part of the great Himalayan (Supplementary fig. 2), highlighting dependency of elevation topography for dry or wet years. However, snow melting (Fig. 5 b and c) mostly shows a reduction upstream of the Himalayas. Its contribution to interannual variability seems less than monsoon rainfall in dry and wet years. Moreover, the pattern did not fit well with the Himalayan rainfall natural variability, which implies snow melting might be a function of the global warming trend (Fig. 5 a).

Local atmospheric conditions and topography significantly modulate rainfall events(Zhang & Liang, 2020). The primary contributor to the precipitation anomalies is atmospheric humidity over the mountain terrain(Smith, 2018; Tao et al., 2020), followed by large-scale circulation via the tropical ocean. Thermal structure climatology (Supplementary Fig. 3(a)-(d)) suggests atmospheric variables influenced by the topographic elevation of the Himalaya. Composite analysis reveals that warming temperature anomalies with increased relative humidity and MSE are responsible for wet years (Supplementary Fig. 3(e) to (g)). Conversely, cooling temperature anomalies with declined relative humidity and MSE are responsible for dry years (Supplementary Fig. 3(i) to (k)). Usually, environmental moist static energy enhances buoyancy. Also, We found moist buoyancy upward over the steep topography during wet years and downward during dry years (Supplementary Fig. 3(h) to (l)). This suggests the need to employ the moist dynamics analysis to interpret correctly. We found a distinctive

anomalous MFC pattern in a cross-section at 94°E (as shown in figure 6a and d) at a lower level from valley to upslope terrain. This anomalous MFC shows an increased anomaly in wet years while a reduction in dry years. The beauty of this 3-dimension MFC is we can diagnose a cross-section to comprehend the vertical distribution and control of the elevation configuration. Furthermore, we decompose MFC in the dynamical and thermodynamical parts, which relate to the circulation effectand the moisture effect, respectively. Most of these changes are contributed by dynamical MFC (figure 6c-d), which suggests an essential role of circulation. Likewise, Thermodynamical MFC (figure 6e-f) shows a similar agreement dominated over slope terrain. The anomalous MFC clearly indicates an enhancement of processes between the surface to 500 hPa, underscoring the role of moisture. However, it should be noted that thermodynamical MFC is nearly ten times smaller in magnitude as compared to dynamical MFC. These results reveal that dynamical MFC modulates rainfall anomalies in the steep terrain of the Himalayas.

The Indian monsoon is modulated by interannual climate mode features such as El Niño–Southern Oscillation (ENSO)(Jian et al., 2009), Indian Ocean dipole (IOD)(Saji et al., 1999), Atlantic Niño (AN)(Sahoo & Yadav, 2021; Zebiak, 1993). Tropical SST condition has been examined for composite dry and wet years. It shows (Supplementary Fig 7) that Himalayan interannual fluctuation can be associated with combined variability patterns in the Atlantic and Indo-Pacific. Positive Atlantic Niño, Negative Indian Ocean Dipole, and La Niña conditions seem favorable for Wet monsoons. A recent teleconnection study also found that Atlantic Nino enhances the MFC over northeast India(Sahoo & Yadav, 2021). Negative Atlantic Niño, Indian Ocean cooling, and neutral Pacific conditions seem favorable for dry monsoons. We illustrated local monsoonal Hadley circulation to understand large-scale circulation linkage with dynamical MFC for dry and wet years. This meridional mean overturning circulation consists of an ascending branch of warm moist air commonly known as a tropical rain belt or Intertropical Convergence Zone (ITCZ). The shift in ITCZ can influence Himayalan rainfall variability. Therefore, we also investigate the its location and associated width(Byrne and Schneider, 2016) as given in Supplementary Table S1. The ITCZ location shifted by 0.47° latitude to the Northward(Hari et al., 2020) with the narrowing of ITCZ width during wet years. The ITCZ location is almost the same as the 43-year climatological mean, with the widening of ITCZ width during wet years. Moreover, the counterclockwise rotation during wet years is stronger than in dry years. As a result, the mean local Hadley cell is narrow during wet years and extends wider during dry years. However, the atmospheric tropical bridge is more important than the background tropical ocean SST anomalies. Zonal Walker circulation and the meridional This is because Walker circulation(Bjerknes, 1969) links these ocean basins and has an ascending branch of the zonal and meridional circulation merged over Maritime Continent. Hadley circulations are connected locally (Karnauskas and Ummenhofer, 2014; Liu and Zhou, 2017; Ma et al., 2018; Yun et al., 2021). Here, we expect a physical linkage between a local headly cell with walker circulation, which reflects rainfall anomalies in the Himalayan region. Walker circulation climatology is represented (see Figure 9a and b; black vectors) during JJAS, An

ascending branch over the Indo-Pacific warm pool, and the Eastern Pacific sector and African landmass. The most dominant vertical velocity anomaly can be found near the Indo-Pacific warm pool region in wet years (Figure 9a)—amplified ascending anomalies in the Eastern Indian Ocean and reduced anomalies over Western Pacific. Conversely, in the case of dry years (Figure 9b), increased ascending anomalies were observed in the Western Pacific Ocean and reduced anomalies Eastern Indian Ocean. These results from the composite analysis suggest that anomalous Walker circulation feeds the local Hadley circulation, which impacts precipitation in the Eastern Himalayan region.

5 Conclusions

To conclude, here we found a strong interannual variability signal in the Eastern Himalayan ranges over steep relief and dominated over south-facing slopes. Himalayan monsoon rainfall has complexity due to its orographic features. Our work suggests this Himalayan variability has two phases, which are responsible for the wetting and drying Himalayan hydroclimate. Additionally, we did not capture any snow melting contribution in interannual variability, underscoring its minor role in river discharge. The Brahmaputra seems more significantly impacted during amplified monsoonal wet years in the Himalayas are favorable for flood risk downstream. The flooding in this region can be the ultimate red alert for Humanity and our ecosystem(Elsen et al., 2020), and threats like degradation of soil(Borrelli et al., 2020) and biodiversity loss(Peters et al., 2019). Composite analysis reveals that moist-orographic features enormously modulate variation patterns through moist processes. A dynamical MFC has been leading in the Himalayan monsoon rainfall variability, also supported by moist buoyancy and relative shift in ITCZ. Our investigation underscores the association between rainfall variability and anomalous convection over Indo-Pacific warm pool driven by local head circulation. This study can be helpful in the predictability of Himalayan rainfall variability and extremes. Even though our study emphasizes natural variability, there is a need to explore in detail the role of climate change as a further study. The Indo-Pacific warm pool(M. K. Roxy et al., 2019; Weller et al., 2016) is expanding substantially under global warming, which could favor more flooding events in Himalayan rivers. The Brahmaputra and Ganges merge in Bangladesh and flow into the Bay of Bengal. This natural variability would have its signature in the Bay of Bengal, which might be fascinating to explore further.

Acknowledgments

The authors wish to acknowledge the use of the PyFerret program for analysis and graphics in this paper. PyFerret is a product of NOAA's Pacific Marine Environmental Laboratory (Information is available at https://ferret.pmel.noaa.gov/Ferret/).

Funding

This work was supported by the National Research Foundation of Korea (NRF) grant funded by the Korean government (MSIT) (Grant No. 2020R1A2C2006860).

Author contributions:

PK and KH conceived the study and wrote the draft manuscript. PK performed the analysis, prepared all figures and wrote the initial draft of the manuscript. Both authors contributed to the interpretation of the results, discussion of the associated mechanisms, and refinement of the paper.

Data Availability Statement:

ERA5 reanalysis data is publicly available from the ECMWF on their Climate Data Store (CDS), https://cds.climate.copernicus.eu/cdsapp#!/home

HadSST data are available at the Met Office Hadley Centre website, https://www.metoffice.gov.uk/hadobs/hadisst/

Earth topography five-minute grid (etopo5) is publicly available at National Geophysical Data Center, https://www.ngdc.noaa.gov/mgg/global/etopo5.HTML

Multi-Source Weighted-Ensemble Precipitation (MSWEP) rainfall product data from GloH2O is publicly available, http://www.gloh2o.org/mswep/

The GloFAS-ERA5 river discharge reanalysis product is publicly available on the CDS, https://cds.climate.copernicus.eu/cdsapp#!/dataset/cems-glofas-historical?tab=overview

The global population density estimates in 2020 from the Gridded Population of the World version 4 (GPWv4), https://sedac.ciesin.columbia.edu/data/set/gpw-v4-population-density-rev11

References

Beck, H. E., Wood, E. F., Pan, M., Fisher, C. K., Miralles, D. G., van Dijk, A. I. J. M., et al. (2019). MSWep v2 Global 3-hourly 0.1° precipitation: Methodology and quantitative assessment. *Bulletin of the American Meteorological Society*, *100*(3). https://doi.org/10.1175/BAMS-D-17-0138.1

Besse, J., Courtillot, V., Pozzi, J. P., Westphal, M., & Zhou, Y. X. (1984). Palaeomagnetic estimates of crustal shortening in the Himalayan thrusts and Zangbo suture. *Nature*, *311*(5987). https://doi.org/10.1038/311621a0

Bhatt, B. C., & Nakamura, K. (2006). A climatological-dynamical analysis associated with precipitation around the southern part of the Himalayas. *Journal of Geophysical Research: Atmospheres*, *111*(D2). https://doi.org/10.1029/2005JD006197

Bjerknes, J. (1969). ATMOSPHERIC TELECONNECTIONS FROM THE EQUATORIAL PACIFIC 1. *Monthly Weather Review*, *97*(3). https://doi.org/10.1175/1520-0493(1969)097<0163:atftep>2.3.co;2

Borrelli, P., Robinson, D. A., Panagos, P., Lugato, E., Yang, J. E., Alewell, C., et al. (2020). Land use and climate change impacts on global soil erosion by water (2015-2070). *Proceedings of the National Academy of Sciences of the United States of America*, *117*(36). https://doi.org/10.1073/pnas.2001403117

Chen, Y., Sharma, S., Zhou, X., Yang, K., Li, X., Niu, X., et al. (2021). Spatial performance of multiple reanalysis precipitation datasets on the southern slope of central Himalaya. *Atmospheric Research*, *250*. https://doi.org/10.1016/j.atmosres.2020.105365

CIESIN. (2018). Gridded Population of the World, Version 4 (GPWv4): Basic Characteristics, Revision 11. Palisades, NY: NASA Socioeconomic Data and Applications Center (SEDAC). *Columbia University Center for International Earth Science Information Network (CIESIN) - Columbia University*.

Elsen, P. R., Monahan, W. B., & Merenlender, A. M. (2020). Topography and human pressure in mountain ranges alter expected species responses to climate change. *Nature Communications*, *11*(1). https://doi.org/10.1038/s41467-020-15881-x

Guo, D., Yu, E., & Wang, H. (2016). Will the tibetan plateau warming depend on elevation in the future? *Journal of Geophysical Research*, *121*(8). https://doi.org/10.1002/2016JD024871

Guo, D., Pepin, N., Yang, K., Sun, J., & Li, D. (2021). Local changes in snow depth dominate the evolving pattern of elevation-dependent warming on the Tibetan Plateau. *Science Bulletin*, *66*(11). https://doi.org/10.1016/j.scib.2021.02.013

Hari, V., Villarini, G., Karmakar, S., Wilcox, L. J., & Collins, M. (2020). Northward Propagation of the Intertropical Convergence Zone and Strengthening of Indian Summer Monsoon Rainfall. *Geophysical Research Letters*, *47*(23). https://doi.org/10.1029/2020GL089823

Harrigan, S., Zsoter, E., Alfieri, L., Prudhomme, C., Salamon, P., Wetterhall, F., et al. (2020). GloFAS-ERA5 operational global river discharge reanalysis 1979-present. *Earth System Science Data*, *12*(3), 2043–2060. https://doi.org/10.5194/essd-12-2043-2020

Hersbach, H., Bell, B., Berrisford, P., Hirahara, S., Horányi, A., Muñoz-Sabater, J., et al. (2020). The ERA5 global reanalysis. *Quarterly Journal of the Royal Meteorological Society*, *146*(730). https://doi.org/10.1002/qj.3803

Hock, R., Rasul, G., Adler, C., Cáceres, B., Gruber, S., Hirabayashi, Y., et al. (2019). Chapter 2: High Mountain Areas. IPCC Special Report on the Ocean and Cryosphere in a Changing Climate. In *IPCC Special Report on the Ocean and Cryosphere in a Changing Climate*.

Hunt, K. M. R., Turner, A. G., & Schiemann, R. K. H. (2022). Katabatic and convective processes drive two preferred peaks in the precipitation diurnal cycle over the Central Himalaya. *Quarterly Journal of the Royal Meteorological Society*, *148*(745). https://doi.org/10.1002/qj.4275

Immerzeel, W. W., Lutz, A. F., Andrade, M., Bahl, A., Biemans, H., Bolch, T., et al. (2020). Importance and vulnerability of the world's water towers. *Nature*, *577*(7790), 364–369. https://doi.org/10.1038/s41586-019-1822-y

Jian, J., Webster, P. J., & Hoyos, C. D. (2009). Large-scale controls on Ganges and Brahmaputra river discharge on intraseasonal and seasonal times-cales. *Quarterly Journal of the Royal Meteorological Society*, *135*(639). https://doi.org/10.1002/qj.384

Karnauskas, K. B., & Ummenhofer, C. C. (2014). On the dynamics of the Hadley circulation and subtropical drying. *Climate Dynamics*, *42*(9–10). https://doi.org/10.1007/s00382-014-2129-1

Kuttippurath, J., Murasingh, S., Stott, P. A., Balan Sarojini, B., Jha, M. K., Kumar, P., et al. (2021). Observed rainfall changes in the past century (1901–2019) over the wettest place on Earth. *Environmental Research Letters*, *16*(2). https://doi.org/10.1088/1748-9326/abcf78

Liu, B., & Zhou, T. (2017). Atmospheric footprint of the recent warming slowdown. *Scientific Reports*, *7*. https://doi.org/10.1038/srep40947

Ma, J., Chadwick, R., Seo, K. H., Dong, C., Huang, G., Foltz, G. R., & Jiang, J. H. (2018). Responses of the Tropical Atmospheric Circulation to Climate Change and Connection to the Hydrological Cycle. *Annual Review of Earth and Planetary Sciences*. https://doi.org/10.1146/annurev-earth-082517-010102

Mahanta, R., Sarma, D., & Choudhury, A. (2013). Heavy rainfall occurrences in northeast India. *International Journal of Climatology*, *33*(6), 1456–1469. https://doi.org/10.1002/JOC.3526

Maurer, J. M., Schaefer, J. M., Rupper, S., & Corley, A. (2019). Acceleration of ice loss across the Himalayas over the past 40 years. *Science Advances*, *5*(6). https://doi.org/10.1126/sciadv.aav7266

Norris, J., Carvalho, L. M. V., Jones, C., & Cannon, F. (2020). Warming and drying over the central Himalaya caused by an amplification of local mountain circulation. *Npj Climate and Atmospheric Science 2020 3:1*, *3*(1), 1–11. https://doi.org/10.1038/s41612-019-0105-5

Palazzi, E., von Hardenberg, J., Terzago, S., & Provenzale, A. (2015). Precipitation in the Karakoram-Himalaya: a CMIP5 view. *Climate Dynamics*, *45*(1–2), 21–45. https://doi.org/10.1007/S00382-014-2341-Z/FIGURES/4

Pathak, R., Sahany, S., Mishra, S. K., & Dash, S. K. (2019). Precipitation Biases in CMIP5 Models over the South Asian Region. *Scientific Reports 2019 9:1*, *9*(1), 1–13. https://doi.org/10.1038/s41598-019-45907-4

Peixto, J. P., & Oort, A. H. (1984). Physics of climate. *Reviews of Modern Physics*, *56*(3), 365. https://doi.org/10.1103/RevModPhys.56.365

Pepin, N., Bradley, R. S., Diaz, H. F., Baraer, M., Caceres, E. B., Forsythe, N., et al. (2015). Elevation-dependent warming in mountain regions of the world. *Nature Climate Change*. https://doi.org/10.1038/nclimate2563

Peters, M. K., Hemp, A., Appelhans, T., Becker, J. N., Behler, C., Classen, A., et al. (2019). Climate–land-use interactions shape tropical mountain biodiversity and ecosystem functions. *Nature*, *568*(7750). https://doi.org/10.1038/s41586-019-1048-z

Rangwala, I., Miller, J. R., & Xu, M. (2009). Warming in the Tibetan Plateau: Possible influences of the changes in surface water vapor. *Geophysical Research Letters*, *36*(6). https://doi.org/10.1029/2009GL037245

Rao, M. P., Cook, E. R., Cook, B. I., D'Arrigo, R. D., Palmer, J. G., Lall, U., et al. (2020). Seven centuries of reconstructed Brahmaputra River discharge demonstrate underestimated high discharge and flood hazard frequency. *Nature Communications*, *11*(1). https://doi.org/10.1038/s41467-020-19795-6

Roxy, M. K., Dasgupta, P., McPhaden, M. J., Suematsu, T., Zhang, C., & Kim, D. (2019). Twofold expansion of the Indo-Pacific warm pool warps the MJO life cycle. *Nature 2019 575:7784*, *575*(7784), 647–651. https://doi.org/10.1038/s41586-019-1764-4

Roxy, Mathew Koll, Ritika, K., Terray, P., Murtugudde, R., Ashok, K., & Goswami, B. N. (2015). Drying of Indian subcontinent by rapid Indian ocean warming and a weakening land-sea thermal gradient. *Nature Communications*, *6*. https://doi.org/10.1038/ncomms8423

Sabin, T. P., Krishnan, R., Vellore, R., Priya, P., Borgaonkar, H. P., Singh, B. B., & Sagar, A. (2020). Climate change over the himalayas. In *Assessment of Climate Change over the Indian Region: A Report of the Ministry of Earth Sciences (MoES), Government of India*. https://doi.org/10.1007/978-981-15-4327-2_11

Sahoo, M., & Yadav, R. K. (2021). Teleconnection of Atlantic Nino with summer monsoon rainfall over northeast India. *Global and Planetary Change*, *203*. https://doi.org/10.1016/j.gloplacha.2021.103550

Saji, N. H., Goswami, B. N., Vinayachandran, P. N., & Yamagata, T. (1999). A dipole mode in the tropical Indian ocean. *Nature*, *401*(6751). https://doi.org/10.1038/43854

Salunke, P., Jain, S., & Mishra, S. K. (2018). Performance of the CMIP5 models in the simulation of the Himalaya-Tibetan Plateau monsoon. *Theoretical and Applied Climatology 2018 137:1*, *137*(1), 909–928. https://doi.org/10.1007/S00704-018-2644-9

Sandu, I., van Niekerk, A., Shepherd, T. G., Vosper, S. B., Zadra, A., Bacmeister, J., et al. (2019). Impacts of orography on large-scale atmospheric circulation. *Npj Climate and Atmospheric Science*, *2*(1). https://doi.org/10.1038/s41612-019-0065-9

Shukla, T., & Sen, I. S. (2021). Preparing for floods on the Third Pole. *Science*, *372*(6539). https://doi.org/10.1126/science.abh3558

Smith, R. B. (2018). 100 years of progress on mountain meteorology research. *Meteorological Monographs*, *59*. https://doi.org/10.1175/AMSMONOGRAPHS-D-18-0022.1

Tao, W., Huang, G., Lau, W. K. M., Dong, D., Wang, P., & Wen, G. (2020). How can CMIP5 AGCMs' resolution influence precipitation in mountain areas: the Hengduan Mountains? *Climate Dynamics*, *54*(1–2). https://doi.org/10.1007/s00382-019-04993-w

Vecchi, G. A., & Soden, B. J. (2007). Global warming and the weakening of the tropical circulation. *Journal of Climate*, *20*(17). https://doi.org/10.1175/JCLI4258.1

Weller, E., Min, S. K., Cai, W., Zwiers, F. W., Kim, Y. H., & Lee, D. (2016). Human-caused Indo-Pacific warm pool expansion. *Science Advances*, *2*(7). https://doi.org/10.1126/sciadv.1501719

Yin, A. (2006). Cenozoic tectonic evolution of the Himalayan orogen as constrained by along-strike variation of structural geometry, exhumation history, and foreland sedimentation. *Earth-Science Reviews*, *76*(1–2). https://doi.org/10.1016/j.earscirev.2005.05.004

Yun, K. S., Timmermann, A., & Stuecker, M. (2021). Synchronized spatial shifts of Hadley and Walker circulations. *Earth System Dynamics*, *12*(1). https://doi.org/10.5194/esd-12-121-2021

Zandler, H., Haag, I., & Samimi, C. (2019). Evaluation needs and temporal performance differences of gridded precipitation products in peripheral mountain regions. *Scientific Reports*, *9*(1). https://doi.org/10.1038/s41598-019-51666-z

Zebiak, S. E. (1993). Air-sea interaction in the equatorial Atlantic region. *Journal of Climate*, *6*(8). https://doi.org/10.1175/1520-0442(1993)006<1567:AIITEA>2.0.CO;2

Zhang, Y., & Liang, C. (2020). Analysis of Annual and Seasonal Precipitation Variation in the Qinba Mountain area, China. *Scientific Reports*, *10*(1). https://doi.org/10.1038/s41598-020-57743-y

Figures

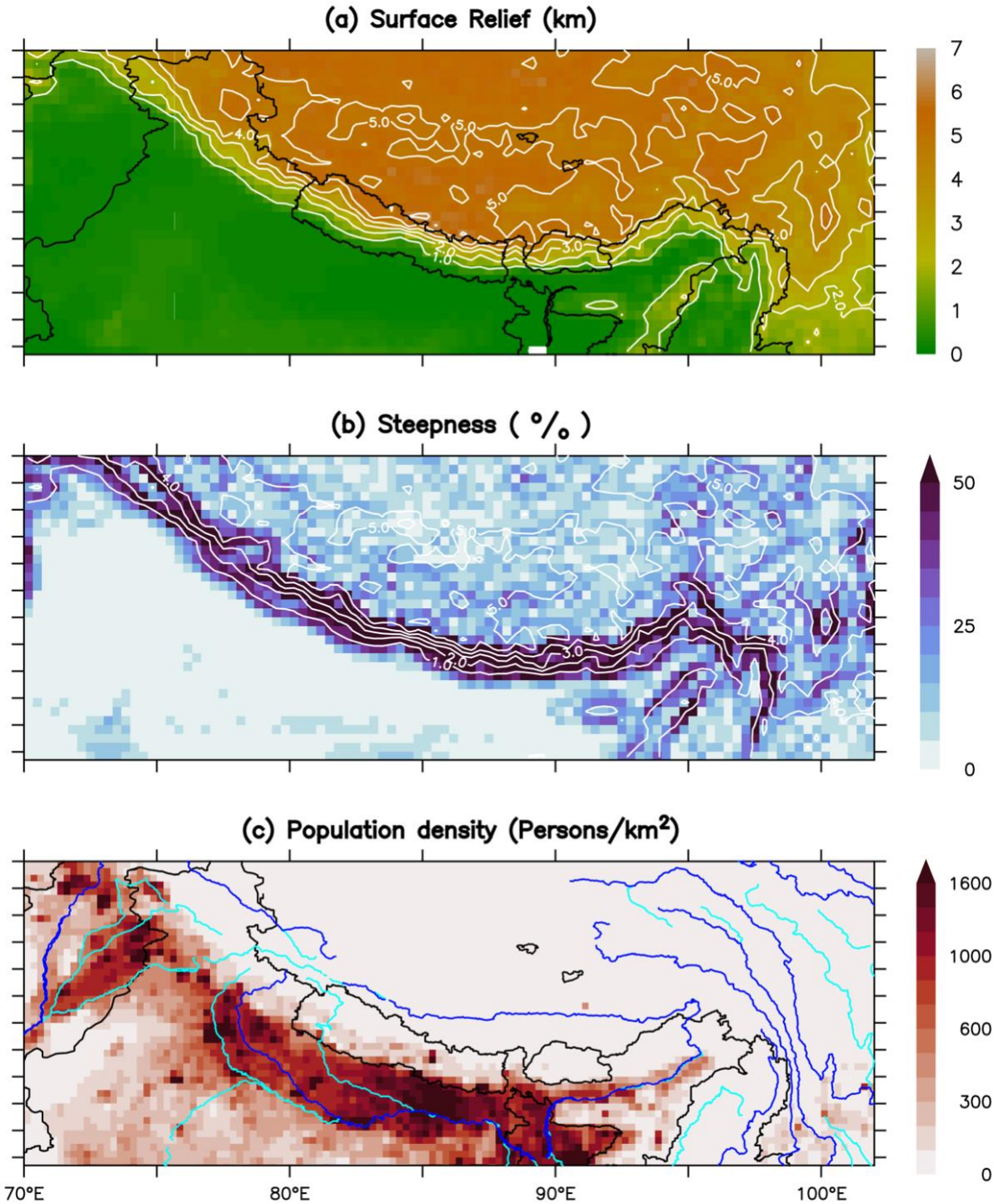

Figure 1. Topographic elevation and demography of the Himalayan region. (a) shaded surface relief (Topography surface of the Earth data at five-minute grid resolution; https://www.ngdc.noaa.gov/mgg/global/etopo5.HTML) with overlayed national borders in black

color and surface relief contour intervals of 1km in white color. (b) Shaded steepness estimated using the slope raster method with surface relief contour intervals of 1km in white color. (c) The shaded population density map highlights the exposed population in 2020 (gridded population of the world version 4 (GPWv4) population density; https://sedac.ciesin.columbia.edu/data/set/gpw-v4-population-density-rev11) overlayed national borders in black color and river system in blue and cyan color.

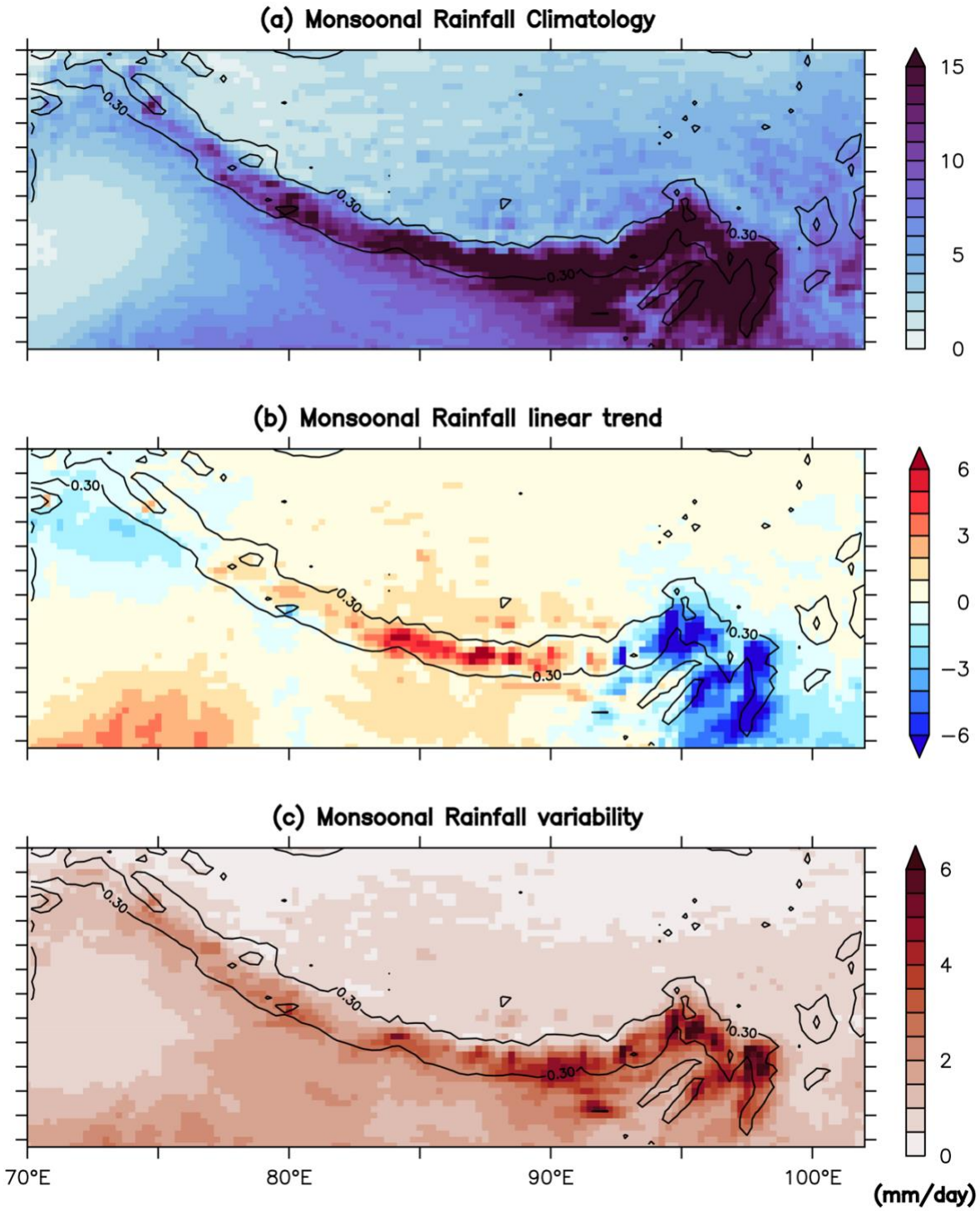

Figure 2. Monsoon seasonal rainfall features over the Himalayan foothills in the last 43 years. (a) Shaded mean rainfall climatology in Himalaya, (b) Shaded trend in rainfall estimated by linear regression method. (c) Shaded rainfall variability in the last 43 years. Here, overlayed white color contours represent regions with elevation steepness higher than 30%.

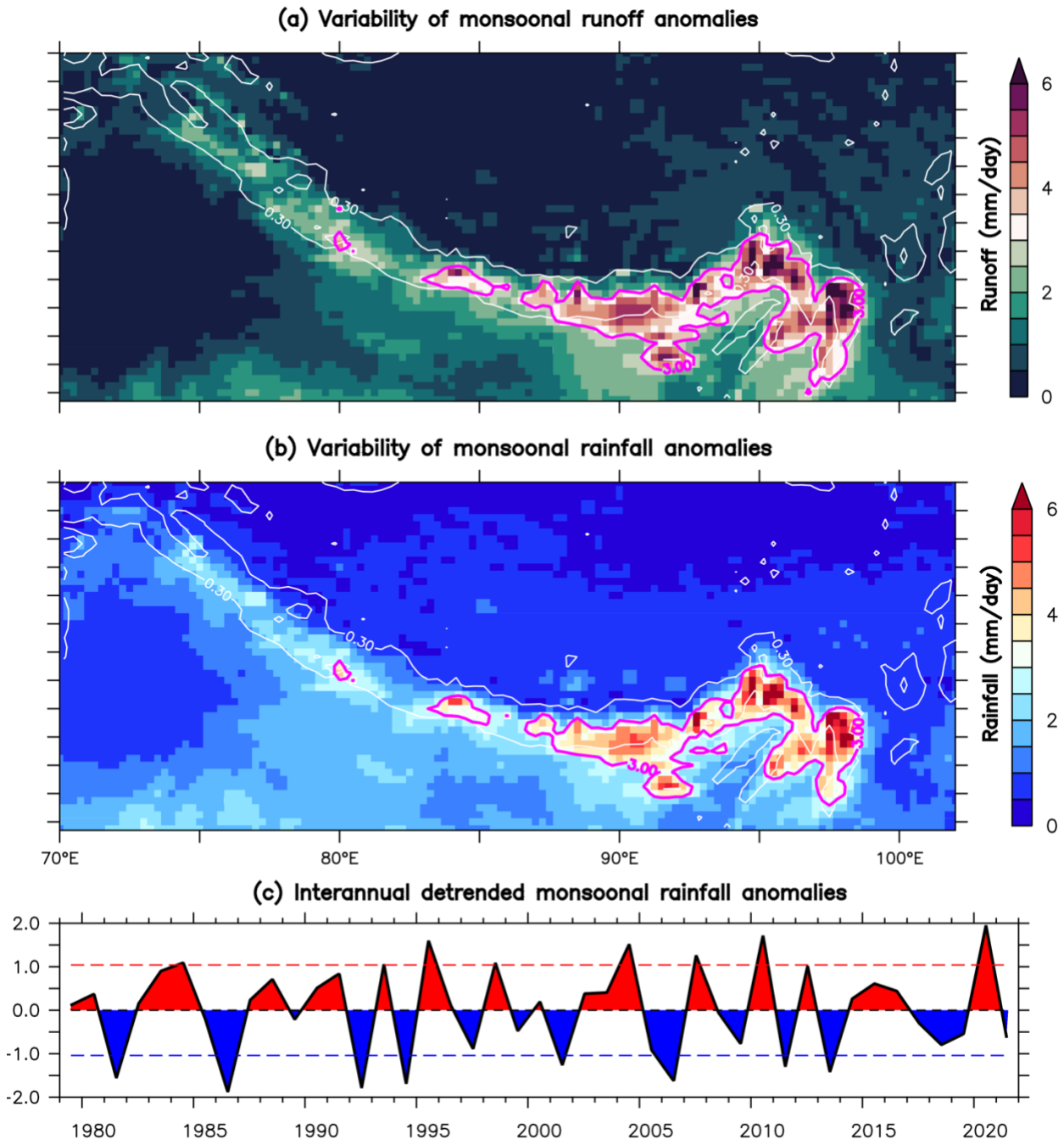

Figure 3. Interannual variability of the Himalayan hydroclimate. (a) Shaded surface relief using the etopo5 dataset with overlayed national borders in black color, river system in blue and cyan color, (b) Interannual amplitude of rainfall anomalies during the last 43 years (1979-2021) from ERA5(Hersbach et al., 2020) (The fifth generation ECMWF reanalysis; https://cds.climate.copernicus.eu/cdsapp#!/home) reanalysis dataset with white contours represent steep topography and black contours denote regions with associated variance more than 3 mm/day consider as high amplitude, and (c) Time series of the linearly detrended monsoonal rainfall

anomalies illustrated in plot, those are normalized with associated multi-year standard deviation. Shaded red (blue) indicates extreme wet (dry) monsoon years. Here we have considered years greater than the multi-year standard deviation (dashed line) of rainfall anomalies for further composite analysis.

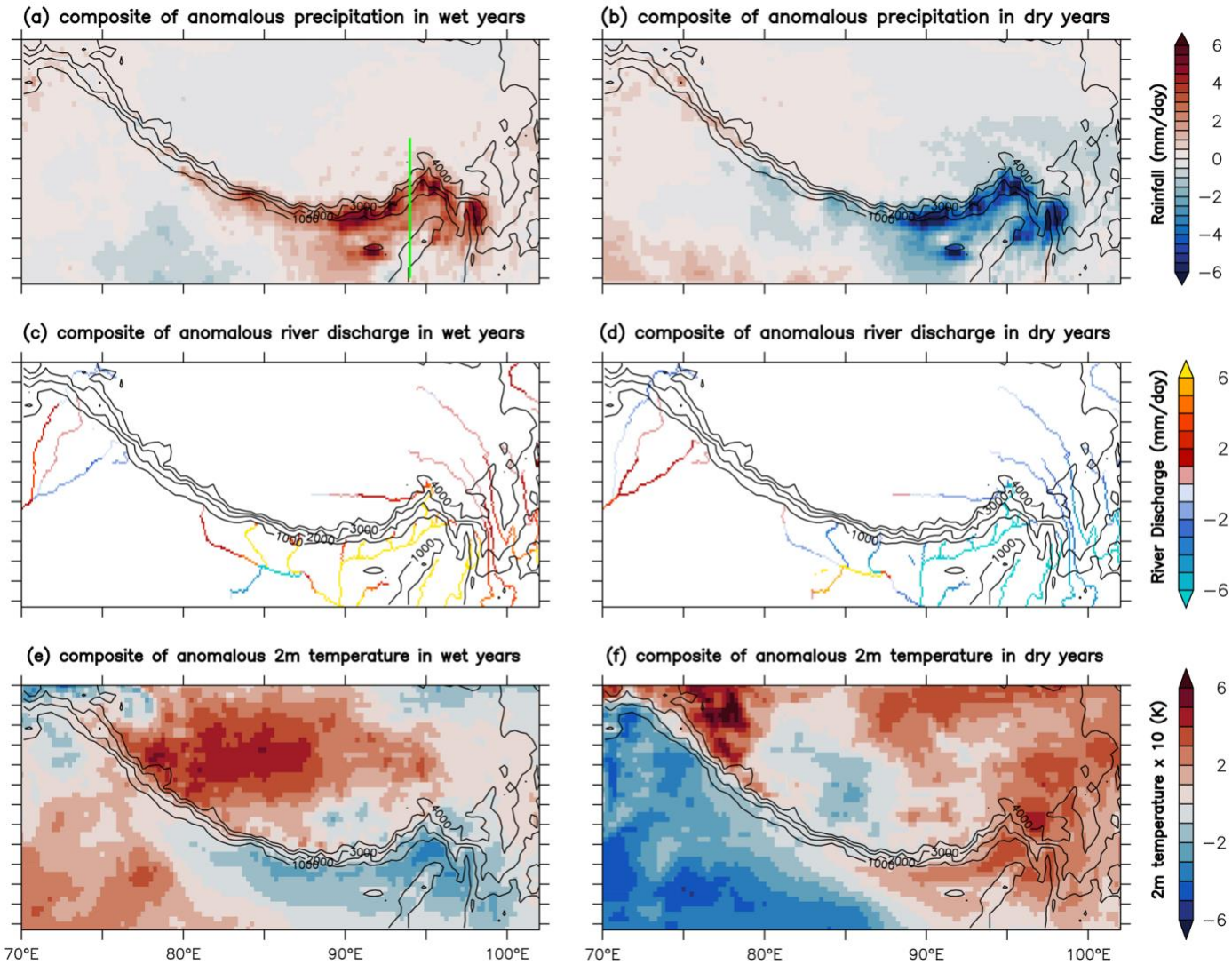

Figure 4. Composite analysis for monsoonal hydroclimate during 1979–2021. (a) Composite map of rainfall anomalies for wet years and (c) dry monsoon years using ERA5(Hersbach et al., 2020) dataset. (c) Composite map of mean river discharge anomalies for wet and (d) dry years using GloFAS-ERA5(Harrigan et al., 2020) (The GloFAS-ERA5 operational global river discharge dataset obtained from https://cds.climate.copernicus.eu/cdsapp#!/dataset/cems-glofas-historical?tab=form) reanalysis). (e) Composite map of 2 m air temperature anomalies for wet and (f) dry years, multiply by 10 factor. Here black contour represents surface relief intervals from 4000 to 1000 m.

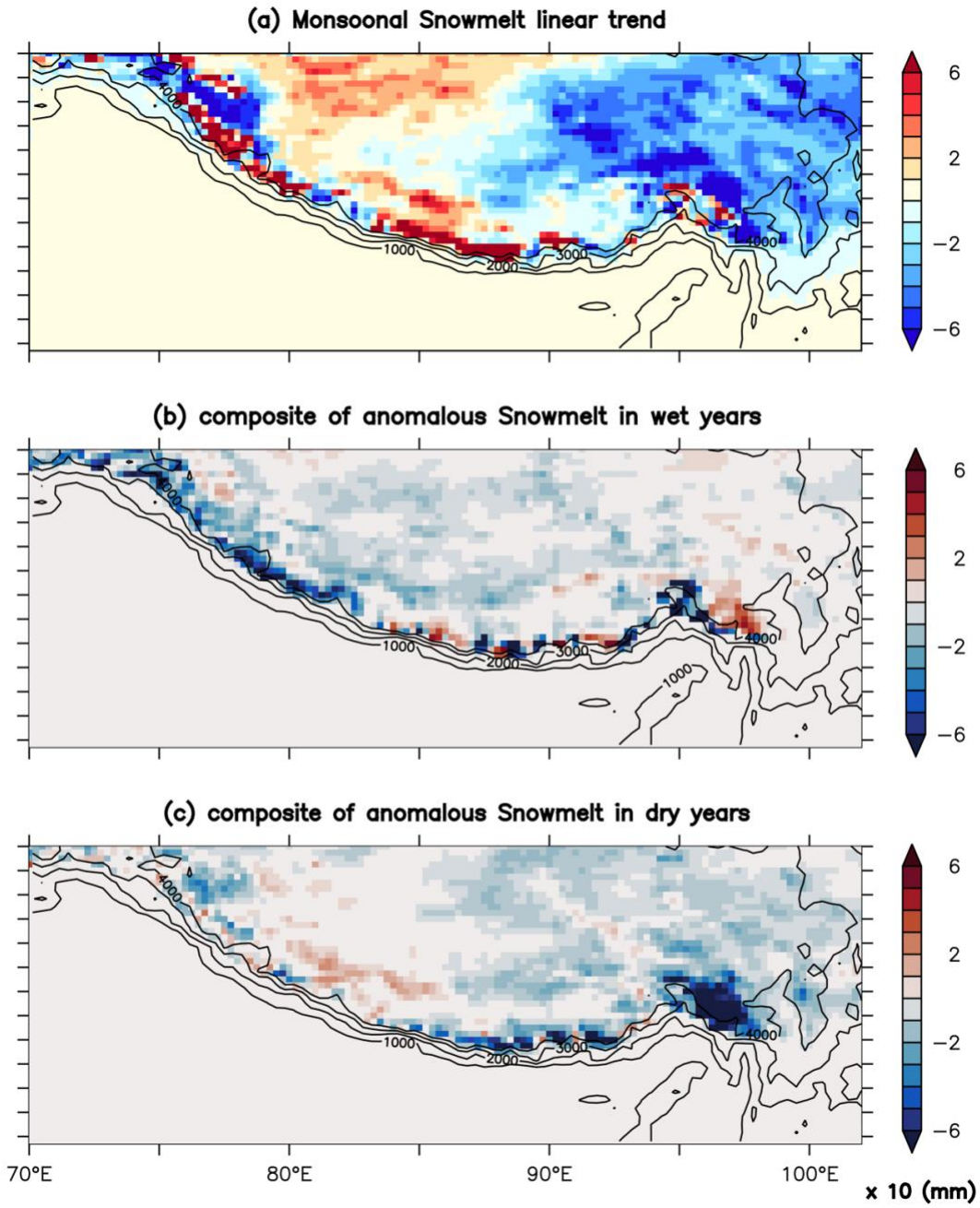

Figure 5. Composite map of snowmelt anomalies for wet and dry monsoon years. Shaded snowmelt (multiplied by 10) with surface relief contour intervals of 1km and white contour intervals denotes steepness. (a) Shaded trend in snowmelt estimated by linear regression method, (b) Composite map of anomalous snowmelt for wet years and and (c) dry monsoon years.

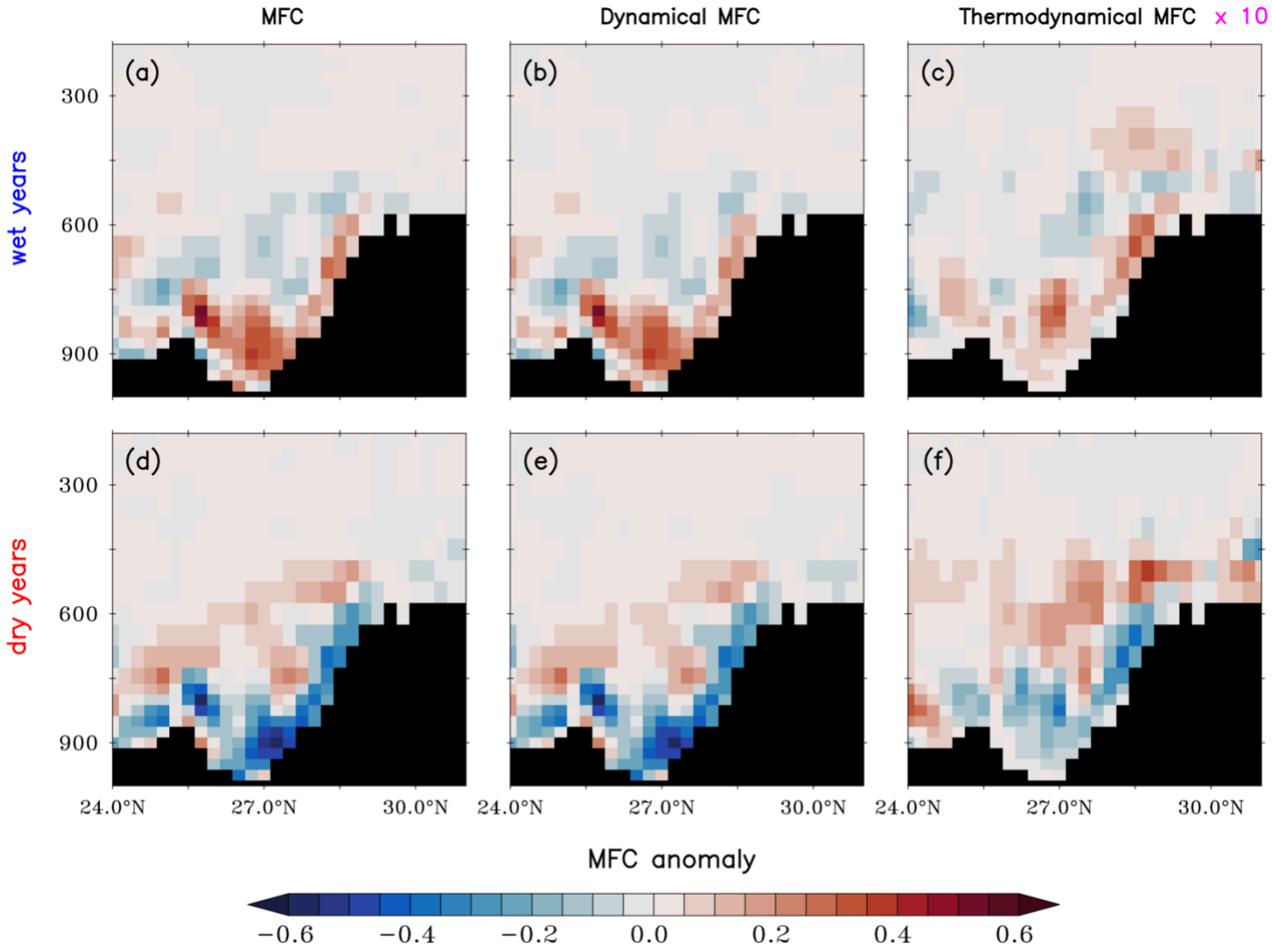

Figure 6. Anomalous moisture flux convergence for composite wet and dry monsoons. Cross section taken over the green line represented in Fig 4 (a) where shaded quantities are moisture flux convergence, dynamical moisture flux convergence, and thermodynamical moisture flux convergence. (a)-(c) for composite wet years, and (b)-(f) for dry years respectively. Where thermodynamical moisture flux convergence is is multiplied by 10. Here, elevation topography regions are masked by black color.

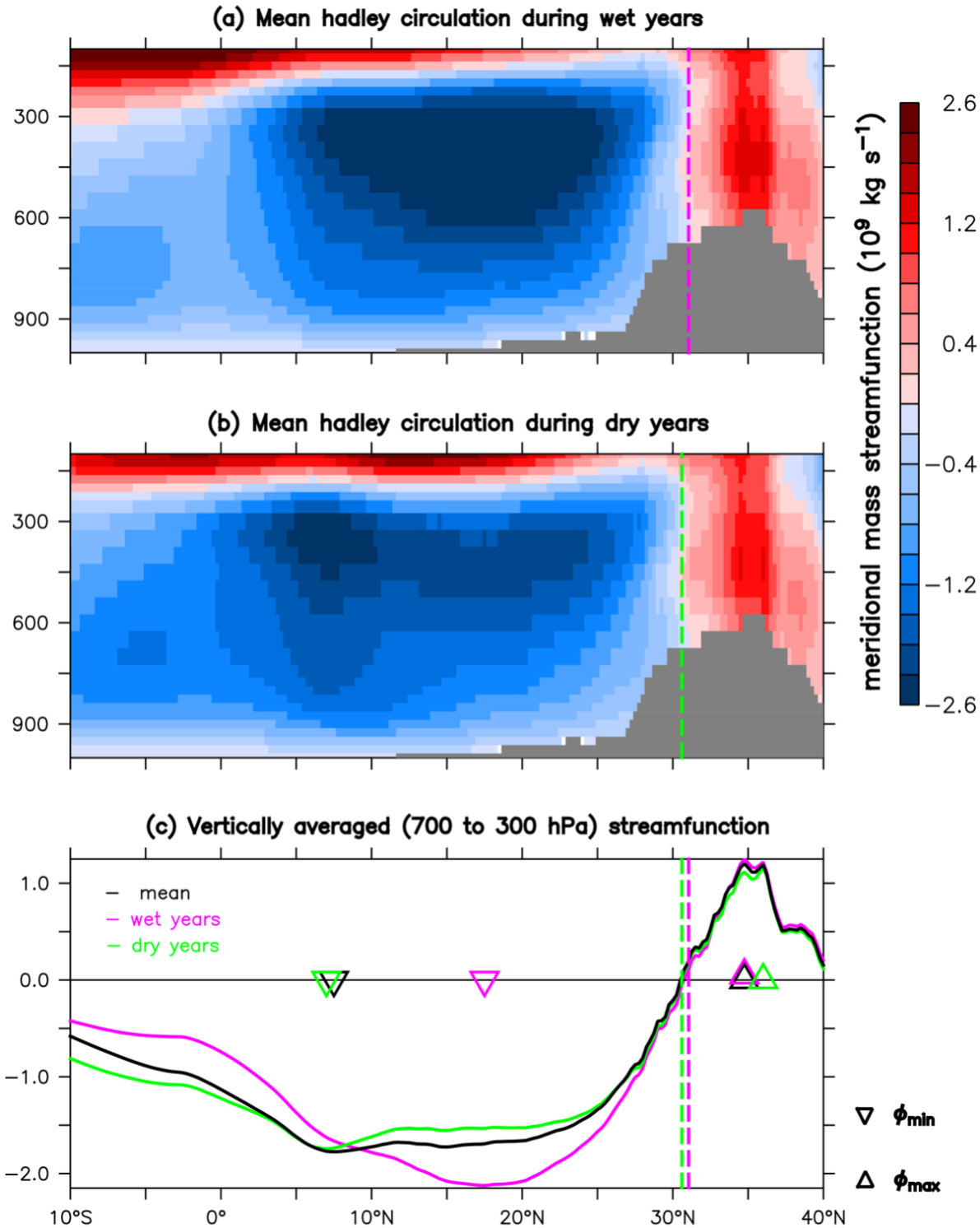

Figure 7. Mean local Hadley circulation in wet and dry monsoon years. Zonal mean meridional Mass stream function averaged over 70°E to 102°E represents local monsoonal circulation (a) for composite wet year and (b) for dry year respectively. A negative (Positive) values of streamfunction indicates counterclockwise (clockwise) circulation. Here, the elevation topography

(averaged over 70°E to 102°E) regions are masked by grey color. (c) Vertically averaged (from 700 hPa to 300 hPa) zonal mean meridional streamfunction. The dashed line shows the location of ITCZ; Maxima and minima latitudinal points are represented with upper and lower empty triangles, respectively.

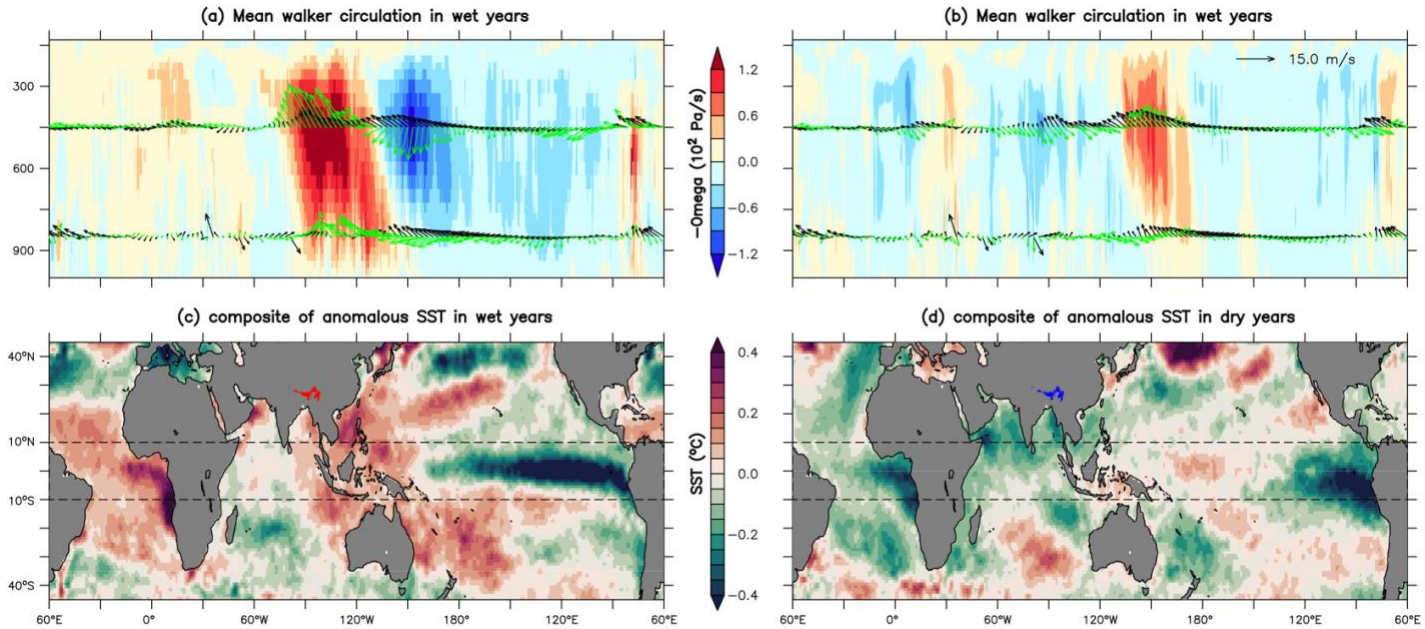

Figure 8. Mean global Walker circulation in wet and dry monsoon years with their composite SST anomalies. Anomalous omega (multiplied by −100) averaged over 10°S–10°N is shaded (a) for a composite wet year and (b) for a dry year, respectively. The black vector represented the composite climatology of wind vectors, while the green vectors showed anomalous wind vectors (multiplied by 10). SST anomalies (c) for wet and (d) dry years using HadSST. Here, the dashed line shows the region consider for Walker circulation.

Supporting Information for

Recent tangible interannual variability of monsoonal orographic rainfall in the Eastern Himalayas

Pratik Kad[1], and Kyung-Ja Ha[1,2,3]

[1]Department of Climate System, Pusan National University, Busan, South Korea

[2]Center for Climate Physics, Institute for Basic Science, Busan, South Korea

[3]BK21 School of Earth and Environmental Systems, Pusan National University, Busan, South Korea

Contents of this file

Supplementary Methods
Figures S1 to S3
Tables S1
Supplementary References

Supplementary Methods

Moist static energy

The moist static energy is used as a thermodynamic variable, which represents the addition of dry static energy and latent energy as:

$$h = C_p T + gz + L_v q$$

where C_p is the specific heat at constant pressure, g is the gravitational constant, z is the height above the surface, and L_v is the latent heat of vaporization.

Buoyancy diagnostics

The moist air parcel buoyancy approach has been taken from previous work(Pascale et al., 2017). To evaluate changes in the atmospheric convective instability, we calculate the buoyancy index(Fu et al., 2021; Pascale et al., 2017; Randall, 2015) at each horizontal grid point with a vertical level.

$$b = \frac{(h_{10m} - h_{env})}{2}$$

Where $h_{10m} = C_p T_{10m} + gz_{10m} + L_v q_{10m}$ is moist static energy at a surface 10m and h_{env} is the environmental saturation moist static energy.

The anomalous buoyancy index Δb is taken with respect to mean state climatology. Positive values indicate upward, and negative values indicate downward acceleration.

ITCZ location

ITCZ location(Byrne & Schneider, 2016) is defined as the latitude closest to the equator where zonal mean streamfunction vertically averaged between 700 and 300 hPa is zero.

$$\phi_{ITCZ} = \phi_{\int \Psi} = 0$$

ITCZ width

The ITCZ width(Byrne & Schneider, 2016) is defined as the latitude distance between the maxima and minima points using the zonal mean streamfunction vertically averaged between 700 and 300.

$$\phi_{\text{width}} = (\phi_{max} - \phi_{\min})$$

Supplementary Figures

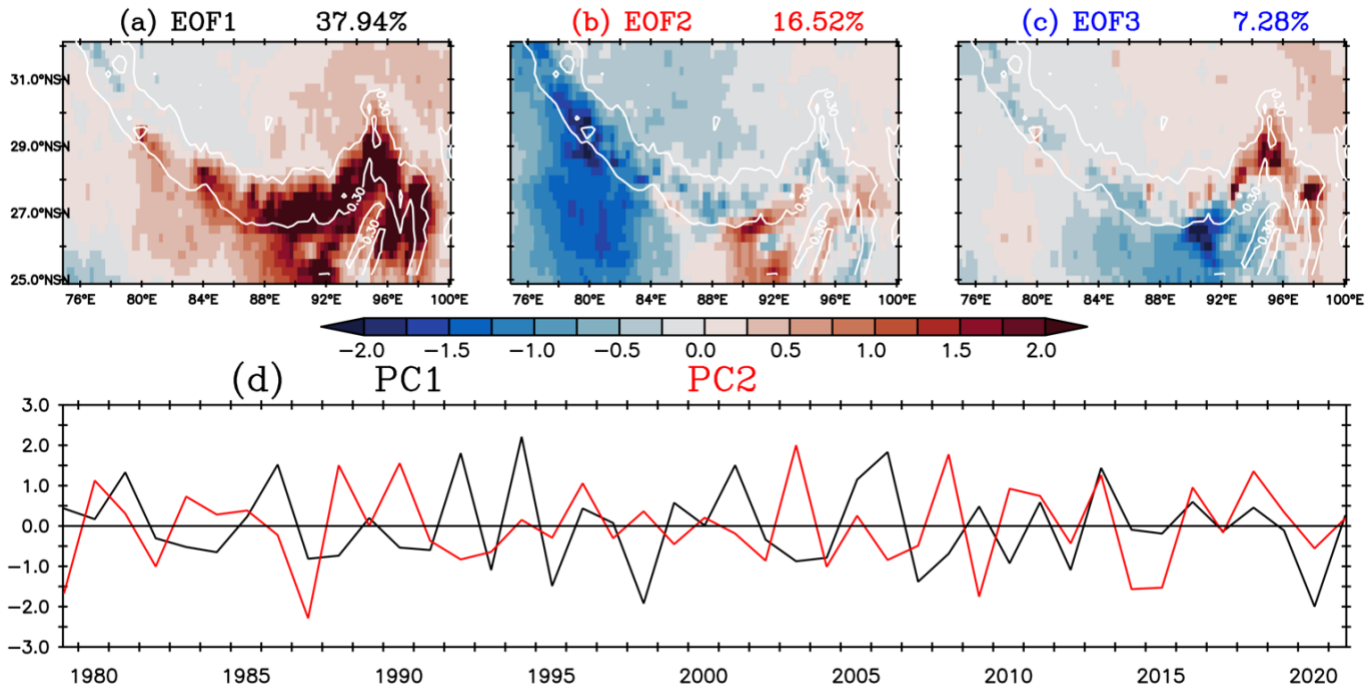

Figure S1. Empirical orthogonal function (EOF) analysis for rainfall. The upper panel shows three dominant EOF modes of Himalayan monsoonal rainfall. The lower panel shows the principal component (PC) time series corresponding to the first and second EOF modes. The leading mode variability (a) suggests high variability, which is compatible with the Eastern Himalayan variability (Main Fig.3).

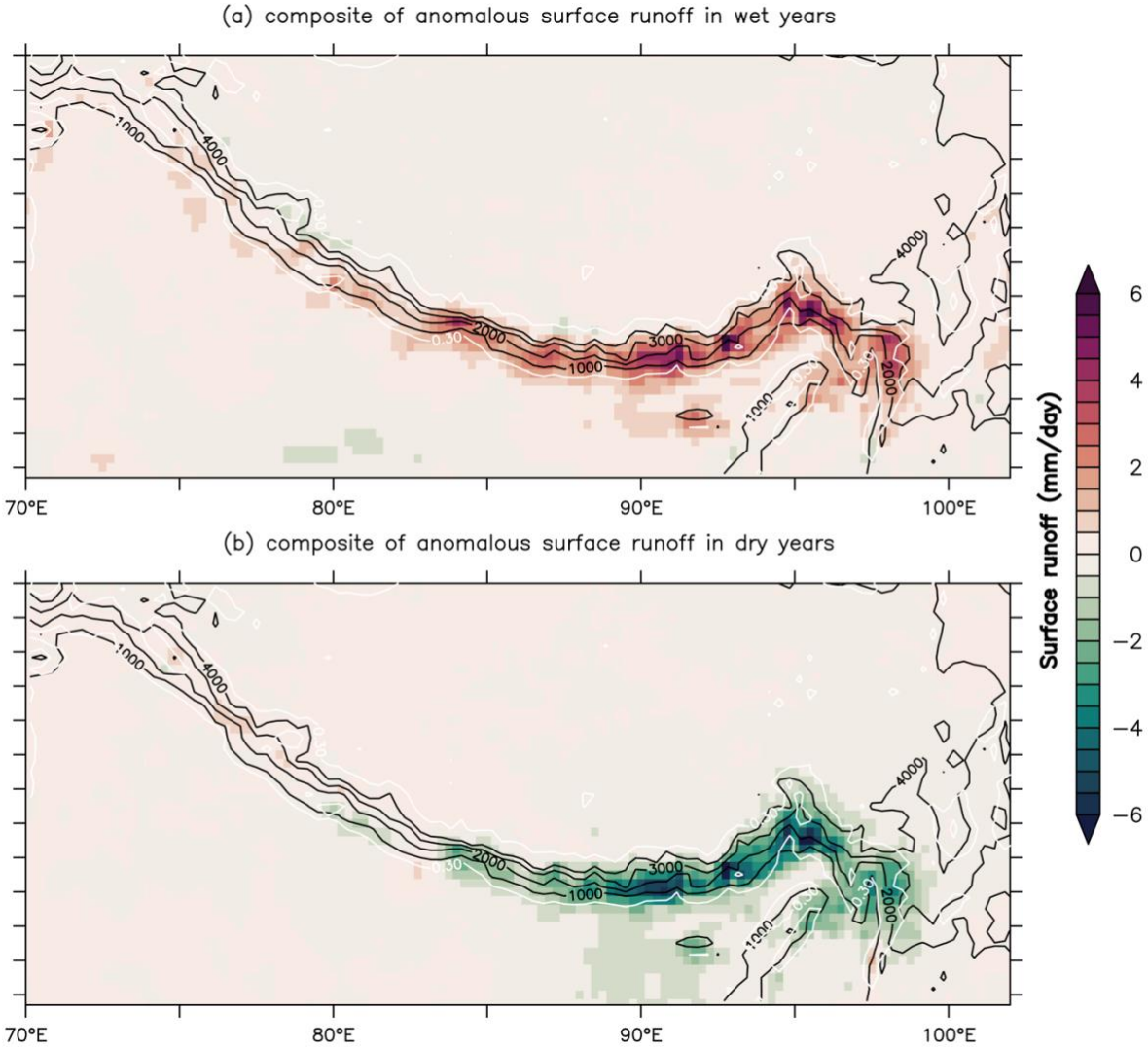

Figure S2. Composite map of surface runoff anomalies for wet and dry monsoon years. (a) Composite map of mean rainfall for wet years and (c) dry monsoon years. Shaded surface runoff with surface relief contour intervals of 1km and white contour intervals denotes steepness.

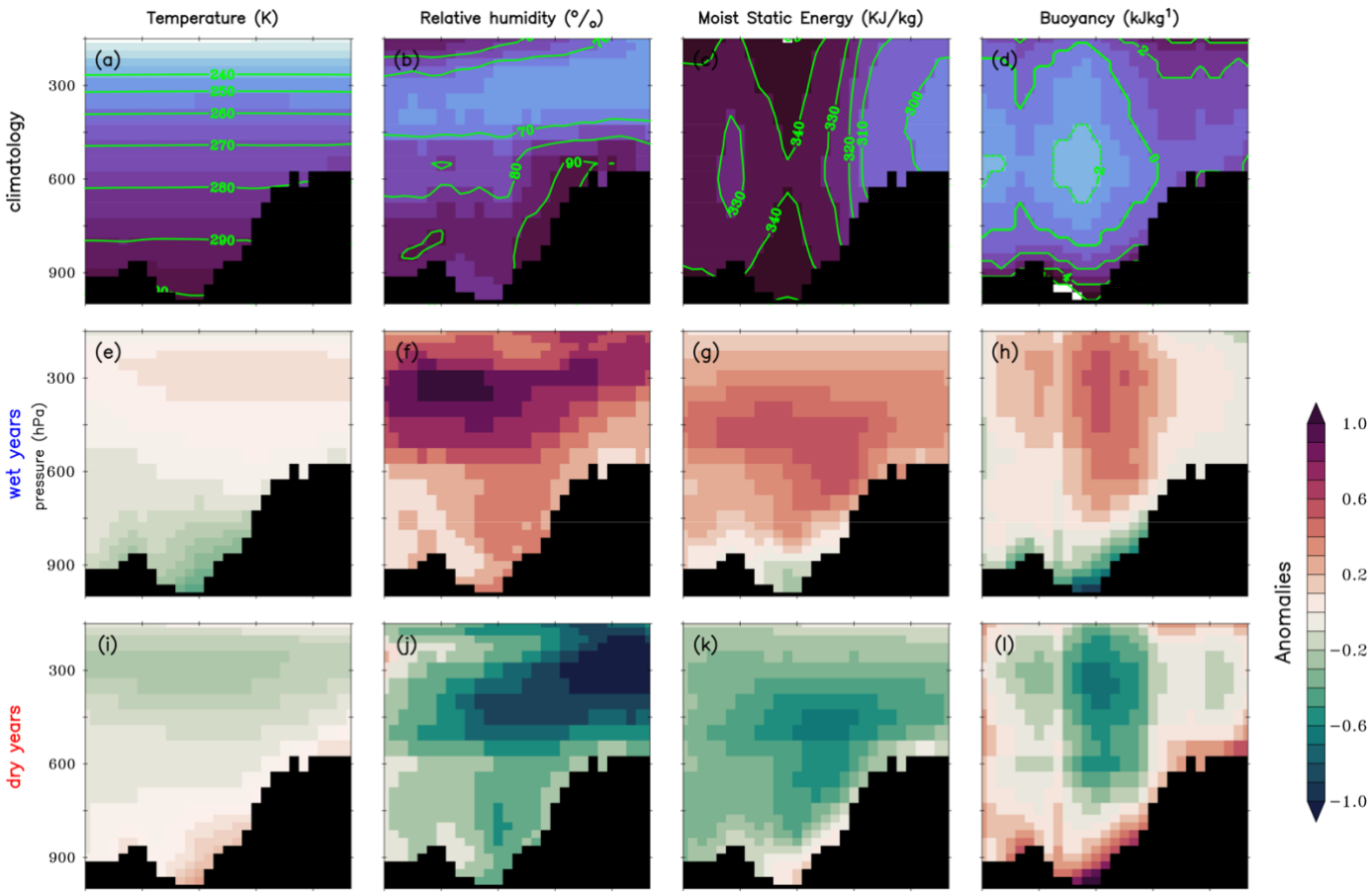

Figure S3. Thermal structure of mean monsoon state climatology, composite anomalies wet and dry monsoons. Cross section taken over green line represented in Fig 4 (a) where shaded quantities are temperature, relative humidity, moist static energy, and buoyancy. (a)-(c) for the mean state climatology of parameters with their green contour intervals units, (d)-(f) for composite wet monsoons, and (g)-(i) for dry monsoons respectively. Here, elevation topography region masked by black color.

Supplementary Table

	ITCZ location (°N) ϕ_{ITCZ}	ITCZ width (km) ϕ_{width}
Climatological mean	30.56	2585.29
Wet years (Δ)	31.03 (0.47)	2017.57 (-567.72)
Dry years (Δ)	30.60 (0.04)	2996.36 (411.07)

Table S1. Mean ITCZ feature indicated, Location and Width (For more information please see Figure 7)

Supplementary References

Byrne, M. P., & Schneider, T. (2016). Narrowing of the ITCZ in a warming climate: Physical mechanisms. *Geophysical Research Letters*, *43*(21), 11,350-11,357. https://doi.org/10.1002/2016GL070396

Fu, D., Chang, P., Patricola, C. M., Saravanan, R., Liu, X., & Beck, H. E. (2021). Central American mountains inhibit eastern North Pacific seasonal tropical cyclone activity. *Nature Communications 2021 12:1*, *12*(1), 1–11. https://doi.org/10.1038/s41467-021-24657-w

Pascale, S., Boos, W. R., Bordoni, S., Delworth, T. L., Kapnick, S. B., Murakami, H., et al. (2017). Weakening of the North American monsoon with global warming. *Nature Climate Change 2017 7:11*, *7*(11), 806–812. https://doi.org/10.1038/nclimate3412

Randall, D. A. (David A. (2015). *An introduction to the global circulation of the atmosphere*. Princeton University. Retrieved from https://press.princeton.edu/books/hardcover/9780691148960/an-introduction-to-the-global-circulation-of-the-atmosphere